Fundamental laws of parametric gain in periodic dispersion-managed optical links

Paolo Serena, Alberto Bononi, and Alessandra Orlandini

Dipartimento di Ingegneria dell'Informazione, Università degli Studi di Parma, Via. G. Usberti, 181/A, 43100 Parma, Italy

A general theory of the parametric gain of amplified spontaneous emission (ASE) noise in periodic dispersion-managed (DM) optical links is presented, based on a linearization of the nonlinear Schrödinger equation around a constant-wave input signal. Closed-form expressions are presented of the in-phase and quadrature ASE power spectral densities (PSDs), valid in the limit of infinitely many spans, for a limited total cumulated nonlinear phase and in-line dispersion, a typical case for nonsoliton systems. PSDs are shown to solely depend on the in-line cumulated dispersion and on the so-called DM kernel. Kernel expressions for both typical terrestrial and submarine DM links are provided. By Taylor expanding the kernel in frequency, we introduce a definition of DM map strength that is more appropriate for limited nonlinear phase DM systems with lossy transmission fibers than the standard definition for soliton systems. Various important special cases of PSDs are discussed in detail. Novel insights, to our knowledge, into the effect of a postdispersion-compensating fiber on such PSDs are included. Finally, examples of application of the PSD formulas to the performance evaluation of both on–off keying and differential phase keying modulated systems are provided. © 2007 Optical Society of America

OCIS codes: 060.2330, 190.4410.

1. INTRODUCTION

The performance of ultra-long-haul transmission systems is significantly limited by the amplified spontaneous emission (ASE) noise introduced by the in-line optical amplifiers. Even if the ASE is generated at each amplifier as an additive white Gaussian process on each transmitted signal, its interaction with the signal through a Kerr-induced four-wave mixing mechanism can significantly change both its power spectral density (PSD) and its first-order statistics at the receiver. The ASE PSD normalized with respect to the white case is known as parametric gain[1] (PG).

Numerous attempts have been made to study the nonlinear Schrödinger equation (NLSE) describing the interaction between the transmitted signal and the noise, but the difficulty of treating a nonlinear operation on a nonstationary stochastic process requires the introduction of strong approximations.

Several recent studies[2–4] introduced numerically intensive perturbation methods, which are accurate but lead to limited physical insight. Most PG studies instead deal with the simplest case of a continuous-wave (cw) launched signal and linearize the NLSE around a cw solution at large optical signal-to-noise ratios (OSNRs) at the end of the line.[1,5–12] Since a Gaussian process after a linear filtering remains Gaussian, the problem reduces to finding an expression for the received ASE PSD. The advantage of the cw linear PG model is its simplicity, which leads to great physical insight.

Note in passing that also parametric amplification, which is a way to exploit PG to advantage, is commonly studied by means of a linearization around one or two cw pumps.[13,14]

Several papers based on the cw model deal with the effect of dispersion management on PG,[6,10–12,15] but these are all based on specific system configurations, and it is difficult to derive from them universal rules that apply to any dispersion-managed (DM) system.

This paper extends the cw small-signal PG model originally developed in Serena *et al.*[16] for bit-error-rate (BER) evaluation of phase-modulated systems. The main purpose of the paper is to obtain fundamental laws that allow a comprehension of PG in any DM periodic link. For mathematical convenience, the analysis is carried out in the limit of infinitely many spans, for a limited total cumulated nonlinear phase and in-line dispersion, a typical case for nonsoliton systems. Simulations for a finite number of spans are then used to verify its range of applicability. The analysis yields closed-form expressions of the ASE PSD, which are discussed in detail in various important special cases. PSDs are shown to solely depend on the in-line cumulated dispersion and on the so-called DM kernel. Kernel expressions for both typical terrestrial and submarine DM links are provided. The appearance of modulation instability[1] in any DM system is shown to be simply related to the absolute value of its DM kernel. By Taylor expanding the kernel in frequency, we propose a definition of DM map strength that is more appropriate for limited nonlinear phase DM systems with lossy transmission fibers than the standard definition for soliton systems.[17] Using the concept of equivalent map strength, system parameters in widely different DM physical systems are found that yield identical ASE PSDs. It is found that nonlinearity in the dispersion-compensating fiber (DCF) at the end of each span has the effect of increasing the equivalent strength. Also, the role of the fiber disper-

sion slope is discussed. It is found that the average dispersion slope acts like a scalar multiplier of the input–output system matrix and does not have any effect on PG. Differential dispersion slope, instead, is found to have an appreciable effect only at close-to-zero group-velocity dispersion of the transmission fiber. The impact of a post-compensation fiber at the end of the DM link is also discussed, with emphasis on the key role of the PSD matrix eigenvalues, which represent the envelope of the in-phase and quadrature PSDs for all possible values of the post-compensation fiber dispersion. Finally, examples of application of the PSD formulas to the performance evaluation of both on–off keying (OOK) and differential phase-shift keying (DPSK) modulated systems are provided, which show that the PG linear model is much more successfully applied to DPSK than to OOK.

The paper is organized as follows. In Section 2 a universal closed-form expression of the in-phase and quadrature ASE PSDs holding for any DM link is derived. General PG-related properties of any kernel are derived in Section 3. Section 4 provides kernel expressions for typical terrestrial and submarine DM links. The concept of equivalent map strength is introduced, and examples are provided of coinciding ASE PSDs in DM systems with the same equivalent map strength. Section 5 shows the impact of fiber dispersion slope on the ASE noise. In Section 6 novel insights, to our knowledge, into the effect of a postdispersion-compensating fiber on received ASE PSDs are presented. Section 7 provides examples of application of the proposed PSD formulas to the performance evaluation of both OOK and DPSK modulated systems. Section 8 summarizes the main findings of the paper.

2. THEORY

The NLSE describes the propagation of an electric field $A(z,t)$ at distance z and retarded time t (in engineering notation) as[1,16]

$$\frac{\partial A}{\partial z} = j\frac{\beta_2(z)}{2}\frac{\partial^2 A}{\partial t^2} + \frac{\beta_3(z)}{6}\frac{\partial^3 A}{\partial t^3} - j\gamma(z)|A|^2 A + \frac{g(z)}{2}A + W_A(z,t),$$

(1)

where $\beta_2(z)$ is the local (group-velocity) dispersion parameter; $\beta_3(z)$ is the third-order dispersion coefficient, related to local dispersion slope; $\gamma(z)$ is the local nonlinear index; $g(z) = -\alpha(z) + \Sigma_k G_k \delta(z - z_k)$ is the net logarithmic power gain–attenuation per unit length, where $\alpha(z)$ is the local fiber attenuation, $\delta(.)$ is the Dirac's delta function, and e^{G_k} is the power gain of the kth lumped amplifier of the link placed at $z = z_k$; and $W_A(z_k, t)$ is a zero-mean complex circular Gaussian noise introduced by the kth amplifier, with a white PSD. Equation (1) deals with the ASE component copolarized with the signal.

We can now normalize time to the supporting pulse duration T of a reference digitally modulated signal by letting $\tau = t/T$. We can also normalize the signal $A(z,t)$ to the power at coordinate z, i.e., $A(z,t) = \sqrt{P}U(z,t)\exp[\frac{1}{2}\int_0^z g(x)dx] = \sqrt{Pf(z)}U(z,t)$, where $f(z) \triangleq \exp \times[\int_0^z g(x)dx]$ is the net power gain from input to coordinate z and P is a reference power. Equation (1) thus becomes

$$\frac{\partial U}{\partial z} = j\frac{1}{2L_d}\frac{\partial^2 U}{\partial \tau^2} + \frac{1}{6L_d'}\frac{\partial^3 U}{\partial \tau^3} - j\frac{f(z)}{L_{NL}}|U|^2 U + W_U(z,\tau),$$

(2)

where we introduced[1] the dispersion length $L_d(z) \triangleq T^2/\beta_2(z)$, the slope length $L_d'(z) \triangleq T^3/\beta_3(z)$, and the nonlinear length $L_{NL}(z) \triangleq 1/[\gamma(z)P]$. L_d and L_d' have the sign of β_2 and β_3, respectively.

If the transmitted field is a cw of power P, in the absence of noise the solution of Eq. (2) is $U(z) = \exp[-j\Phi_{NL}(z)]$, where $\Phi_{NL}(z) \triangleq \int_0^z [f(x)/L_{NL}(x)]dx$ is the nonlinear phase cumulated by the cw. By adding the noise contribution, we search for a perturbed solution of Eq. (2) of the kind[1]

$$U(z,\tau) = [1 + u(z,\tau)]\exp[-j\Phi_{NL}(z)],$$

(3)

where $u(z,\tau)$ is a complex perturbation field. By inserting Eq. (3) into Eq. (2), and with the fundamental assumption $|u|^2 \ll 1$ that allows neglecting quadratic and higher-order ASE terms, we obtain the linearized NLSE for the perturbation:

$$\frac{\partial u}{\partial z} = j\frac{1}{2L_d}\frac{\partial^2 u}{\partial \tau^2} + \frac{1}{6L_d'}\frac{\partial^3 u}{\partial \tau^3} - j\frac{f(z)}{L_{NL}}(u + u^*) + W_U,$$

(4)

where the asterisk denotes complex conjugation and the constant phase rotation Φ_{NL} in Eq. (3) does not change the statistics of the circularly symmetric noise W_U. We now indicate the Fourier transforms of $u(z,\tau)$ and $W_U(z,\tau)$ as $\tilde{u}(z,\omega)$ and $\tilde{W}_U(z,\omega)$, respectively, where ω is the angular frequency normalized to $1/T$. Even if such transforms may not exist for stationary stochastic processes, one can always interpret them as the transforms of time-truncated versions of the signals over a suitable time window T_0, which allows one to compute the PSD according to the Wiener–Khinchin theory.[18] Hence, in the frequency domain,

$$\frac{\partial \tilde{u}}{\partial z} = -j\frac{\omega^2}{2L_d(z)}\tilde{u}(z,\omega) - j\frac{\omega^3}{6L_d'(z)}\tilde{u}(z,\omega)$$

$$-j\frac{f(z)}{L_{NL}(z)}[\tilde{u}(z,\omega) + \tilde{u}^*(z,-\omega)] + \tilde{W}_U(z,\omega).$$

(5)

Now assume the link is composed of identical spans of length L, so that $f(z)$, $L_d(z)$, $L_d'(z)$, and $L_{NL}(z)$ are periodic functions, and let $\langle h \rangle \triangleq (1/L)\int_0^L h(x)dx$ indicate the span average of the generic function $h(z)$. Decompose the local dispersion and slope lengths as $1/L_d(z) = (1/L_D) + [1/L_\Delta(z)]$ and $1/L_d'(z) = (1/L_D') + [1/L_\Delta'(z)]$, where $1/L_D \triangleq \langle 1/L_d \rangle$ and $1/L_D' \triangleq \langle 1/L_{d'} \rangle$ are the span-averaged inverse dispersion and slope lengths, respectively. The terms $1/L_\Delta$ and $1/L_\Delta'$ account for the local deviation from such average values. Inside each span, we recognize two different dynamics along z due to the fiber dispersion[10,17]: average or slow dynamics due to L_D, L_D' and fast dynamics due to L_Δ, L_Δ'. We next move into a reference system that follows the fast dynamics by making the change of variable[10,17]:

$$\tilde{u}(z,\omega) = \tilde{a}(z,\omega)\exp\left[-j\frac{\Theta_\Delta(z,\omega)}{2}\right], \qquad (6)$$

where

$$\Theta_\Delta = \omega^2 \int_0^z \left[\frac{1}{L_\Delta(x)} + \frac{\omega}{3L'_\Delta(x)}\right]\mathrm{d}x.$$

Substituting Eq. (6) in Eq. (5) yields

$$\frac{\partial\tilde{a}}{\partial z} = -j\frac{\omega^2}{2L_D}\tilde{a}(z,\omega) - j\frac{\omega^3}{6L_{D'}}\tilde{a}(z,\omega) - j\frac{f(z)}{L_{\mathrm{NL}}(z)}$$

$$\times[\tilde{a}(z,\omega) + \tilde{a}^*(z,-\omega)\exp(j\Theta_\Delta)] + \tilde{W}_U(z,\omega), \qquad (7)$$

where again the phase rotation in Eq. (6) does not change the Gaussian statistics of the noise $\tilde{W}_U$. For a given finite received nonlinear phase, when the number of spans $N_s \to \infty$, the infinitesimal nonlinear phase rotation per span drives the evolution of $\tilde{a}(z,\omega)$ as a slowly varying z function span by span: $\tilde{a}(z,\omega)$ cannot follow the fast variations within each span due to $L_{\mathrm{NL}}(z)$, $f(z)$, and $\Theta_\Delta(z,\omega)$ but rather only their average effect. Hence, by the method of averaging,[19] one substitutes the rapidly z-varying coefficients in Eq. (7) with their span-averaged values. Define the kernel of the transmission link[17] as

$$\mathcal{R}(\omega) \triangleq \left\langle \frac{f(z)e^{j\Theta_\Delta(z,\omega)}}{L_{\mathrm{NL}}(z)} \right\rangle = \frac{1}{L}\int_0^L \frac{f(x)e^{j\Theta_\Delta(x,\omega)}}{L_{\mathrm{NL}}(x)}\mathrm{d}x, \qquad (8)$$

and note that for a link of length z it is $\mathcal{R}(0)z = \Phi_{\mathrm{NL}}$, so that $\mathcal{R}(0)$ is the nonlinear phase rotation per unit length. With the additional definition of the operator $\mathcal{L}(\omega) \triangleq \mathcal{R}(0) + (\omega^2/2L_D) + (\omega^3/6L'_D)$, Eq. (7) becomes, after span averaging of its coefficients,

$$\frac{\partial\tilde{a}}{\partial z} = -j[\mathcal{L}(\omega)\tilde{a}(z,\omega) + \mathcal{R}(\omega)\tilde{a}^*(z,-\omega)] + \tilde{W}(z,\omega), \qquad (9)$$

where, since we treated each span as a differential $\mathrm{d}z$, we substituted the white ASE $\tilde{W}_U$ with a Langevin noise process $\tilde{W}$, completely distributed along z with PSD at coordinates (z_1,z_2) equal to[20]

$$E\{\tilde{W}(z_1,\omega)\tilde{W}^*(z_2,\omega)\} = 2\sigma^2\delta(z_1 - z_2), \qquad (10)$$

with E{.} indicating statistical averaging and $2\sigma^2$ indicating the one-sided ASE PSD per unit length in absence of PG. Note that even if $\tilde{W}$ does not have continuous paths, Eq. (9) makes sense from a mathematical point of view using the Ito interpretation of a stochastic differential equation.[21] Note also that in Eq. (9) the operator $\mathcal{L}$ accounts for the slow dynamics, while $\mathcal{R}$ accounts for the fast dynamics. It can be immediately observed that the slow dynamics are responsible for a phase shift on $\tilde{a}$, while the fast dynamics allow the energy transfer to the noise. A lengthy but straightforward computation shows that Eq. (9) coincides with a linearization of the so-called DM-NLSE[17] (extended to include dispersion slope and in which space z is the only dimensional quantity left) around the ansatz [Eq. (3)].

Decompose now the noise as $\tilde{a}(z,\omega) = \tilde{a}_p(z,\omega) + j\tilde{a}_q(z,\omega)$, where $\tilde{a}_p(z,\omega) = \frac{1}{2}[\tilde{a}(z,\omega) + \tilde{a}^*(z,-\omega)]$ and $\tilde{a}_q(z,\omega) = 1/2j[\tilde{a}(z,\omega) - \tilde{a}^*(z,-\omega)]$ are the (complex) transforms of the (real) noise components $a_p(z,\tau)$ and $a_q(z,\tau)$ in phase and quadrature with the cw signal. Note that $\tilde{a}_p$ is the dominant source of noise in the envelope detection of an OOK signal, while $\tilde{a}_q$ mainly affects phase-modulated signals. Since $\tilde{a}_p$ and $\tilde{a}_q$ are two Hermitian signals, it is useful to similarly decompose the operators $\mathcal{L}$ and $\mathcal{R}$ as $\mathcal{L} = \mathcal{L}_p + j\mathcal{L}_q$ and $\mathcal{R} = \mathcal{R}_p + j\mathcal{R}_q$, having defined $\mathcal{K}_p(\omega) = \frac{1}{2}[\mathcal{K}(\omega) + \mathcal{K}^*(-\omega)]$ and $\mathcal{K}_q(\omega) = 1/2j[\mathcal{K}(\omega) - \mathcal{K}^*(-\omega)]$, where $\mathcal{K}$ stands for either $\mathcal{L}$ or $\mathcal{R}$. Note that $\mathcal{K}_p$ and $\mathcal{K}_q$ are, in general, complex numbers. Explicitly, the slow operator components are

$$\mathcal{L}_p z = \Phi_{\mathrm{NL}} - \frac{\omega^2}{2}\xi_{\mathrm{in}},$$

$$\mathcal{L}_q z = -j\frac{\omega^3}{6}\xi'_{\mathrm{in}}, \qquad (11)$$

where $\xi_{\mathrm{in}} \triangleq -z/L_D$ represents the normalized in-line cumulated dispersion (having the sign of dispersion in picoseconds per nanometer) and where we also introduced the normalized dispersion slope $\xi'_{\mathrm{in}} \triangleq z/L'_D$.

By exploiting the properties of Hermitian signals, we can write Eq. (9) in matrix notation as

$$\frac{\partial\mathbf{a}(z,\omega)}{\partial z} = \mathbf{M}(\omega)\mathbf{a}(z,\omega) + \mathbf{W}(z,\omega), \qquad (12)$$

where $\mathbf{a} = [\tilde{a}_p, \tilde{a}_q]^T$ and $\mathbf{W} = [\tilde{W}_p, \tilde{W}_q]^T$ are column vectors, with ^{T} indicating transposition, and $\mathbf{M} = \mathcal{L}_q\mathbf{I} + \mathbf{A}$ is a 2×2 matrix, with $\mathbf{I}$ as the identity matrix and

$$\mathbf{A} = \begin{bmatrix} \mathcal{R}_q & \mathcal{L}_p - \mathcal{R}_p \\ -\mathcal{L}_p - \mathcal{R}_p & -\mathcal{R}_q \end{bmatrix}.$$

The closed-form solution of Eq. (12) is[19]

$$\mathbf{a}(z,\omega) = e^{\mathbf{M}(\omega)z}\mathbf{a}(0,\omega) + \int_0^z e^{\mathbf{M}(\omega)x}\mathbf{W}(z-x,\omega)\mathrm{d}x. \qquad (13)$$

The autonomous solution, $e^{\mathbf{M}(\omega)z}\mathbf{a}(0,\omega)$, in the absence of ASE, can be used to study the DM system response to an input OOK modulation in the case of a small extinction ratio. However, in this paper we will not pursue this issue, and we will concentrate on the ASE forced solution in the case of a noiseless cw input, $\mathbf{a}(0,\omega) = \mathbf{0}$. The forced solution, the second term in Eq. (13), tells us that the total noise at the link output z is the sum of all white ASE noise contributions generated at the generic distance x from the output, filtered by the system matrix $e^{\mathbf{M}x}$ seen from the generation point to the output. The system matrix $e^{\mathbf{M}z}$ can be evaluated as follows. The traceless matrix $\mathbf{A}$ has eigenvalues $\pm k$, with

$$k = \sqrt{\mathcal{R}_p^2 + \mathcal{R}_q^2 - \mathcal{L}_p^2}. \qquad (14)$$

Using a corollary of the Cayley–Hamilton theorem,[22] we can express $e^{\mathbf{M}z}$ in the form

$$e^{\mathbf{M}z} = e^{\mathcal{L}_q z}\left[\cosh(kz)\mathbf{I} + \frac{\sinh(kz)}{kz}\mathbf{A}z\right], \qquad (15)$$

which clarifies that the system transfer matrix is completely specified by the operators $\mathcal{L}_p, \mathcal{L}_q$ and $\mathcal{R}_p, \mathcal{R}_q$. Note that the small-signal transfer function (15) reveals that the average dispersion slope, expressed by $\mathcal{L}_q$, acts like a scalar multiplier and could thus, in principle, be compensated for by a lumped slope compensator at the end of the link.

Using the Wiener–Khinchin theorem, we can now evaluate the PSD matrix of the output ASE as

$$\mathbf{S}(z,\omega) = \lim_{T_0\to\infty}\frac{\mathrm{E}\{\mathbf{a}(z,\omega)\mathbf{a}^\dagger(z,\omega)\}}{T_0} \triangleq \begin{bmatrix} S_{\mathrm{pp}} & S_{\mathrm{pq}} \\ S_{\mathrm{qp}} & S_{\mathrm{qq}} \end{bmatrix}, \quad (16)$$

where S_{pp} is the PSD of the in-phase component, S_{qq} is the PSD of the quadrature component, and $S_{\mathrm{pq}} = S_{\mathrm{qp}}^*$ is the cross PSD. The symbol $\dagger$ indicates transpose–conjugate. Using $\mathrm{E}[\mathbf{W}(x,\omega)\mathbf{W}^\dagger(y,\omega)] = \sigma^2\delta(x-y)\mathbf{I}$, from Eq. (13), one then gets the PSD normalized to the case without PG as

$$\hat{\mathbf{S}} \triangleq \frac{\mathbf{S}}{\sigma^2 z} = \frac{1}{z}\int_0^z e^{\mathbf{M}x}e^{\mathbf{M}^t x}\mathrm{d}x = \frac{1}{z}\int_0^z e^{\mathbf{A}x}e^{\mathbf{A}^\dagger x}\mathrm{d}x, \qquad (17)$$

where in the last step we used the fact that $\mathcal{L}_q$ is imaginary and thus cancels out. Hence the average dispersion slope effects, which come into play through the scalar multiplier $e^{\mathcal{L}_q z}$, do not affect the PSDs. Using Eq. (15), one gets

$$\hat{\mathbf{S}} = f_1\mathbf{I} + f_2\mathbf{A}\mathbf{A}^\dagger + f_3^*\mathbf{A}z + f_3\mathbf{A}^\dagger z,$$

where

$$f_1 = \frac{1}{z}\int_0^z |\cosh(kx)|^2 dx = \frac{1}{2}\left[\frac{\sinh(2k_r z)}{2k_r z} + \frac{\sin(2k_i z)}{2k_i z}\right],$$

$$f_2 = \frac{1}{z^3}\int_0^z \left|\frac{\sinh(kx)}{k}\right|^2 dx$$

$$= \frac{1}{2|kz|^2}\left[\frac{\sinh(2k_r z)}{2k_r z} - \frac{\sin(2k_i z)}{2k_i z}\right],$$

$$f_3 = \frac{1}{z^2}\int_0^z \frac{\cosh(kx)\sinh(k^*x)}{k^*}dx$$

$$= \frac{1}{2k^*z}\left[\frac{\cosh(2k_r z)-1}{2k_r z} + j\frac{\cos(2k_i z)-1}{2k_i z}\right], \qquad (18)$$

in which $k = k_r + jk_i$, with real k_r, k_i, and clearly f_1, f_2 are real. The normalized PSD matrix entries are

$$\hat{S}_{\mathrm{pp}} = f_1 + f_2(|\mathcal{R}_q|^2 + |\mathcal{L}_p - \mathcal{R}_p|^2)z^2 + 2\Re\{f_3\mathcal{R}_q^*\}z,$$

$$\hat{S}_{\mathrm{qq}} = f_1 + f_2(|\mathcal{R}_q|^2 + |\mathcal{L}_p + \mathcal{R}_p|^2)z^2 - 2\Re\{f_3\mathcal{R}_q^*\}z,$$

$$\hat{S}_{\mathrm{pq}} = -2[\Re\{f_3\mathcal{R}_p^*\}z + f_2\Re\{\mathcal{R}_q\}\mathcal{L}_p z^2 + j(\Im\{f_3\}\mathcal{L}_p z$$
$$+ f_2\Im\{\mathcal{R}_q\mathcal{R}_p^*\}z^2)], \qquad (19)$$

where $\Re\{.\}$ and $\Im\{.\}$ indicate real and imaginary parts of their complex argument. In the limit $\omega\to 0$, the ASE PSD matrix reduces to

$$\hat{\mathbf{S}} = \begin{bmatrix} 1 & -\Phi_{\mathrm{NL}} \\ -\Phi_{\mathrm{NL}} & 1 + \dfrac{4}{3}\Phi_{\mathrm{NL}}^2 \end{bmatrix}, \qquad (20)$$

which clarifies that the quadrature component exhibits an inflation proportional to the square of the nonlinear phase and is an approximation of the nonlinear phase noise.[23] Note that at large nonlinear phases the negative phase–quadrature correlation becomes significant. In the opposite limit we have $\hat{\mathbf{S}}(z,\omega\to\infty) = \mathbf{I}$; i.e., away from the PG region of influence, the PSD is white, as can be directly deduced from Eq. (9), since the kernel $\mathcal{R}(\omega\to\infty) \to 0$.

3. GENERAL KERNEL PROPERTIES

We now focus our discussion on the kernel for the general DM link shown in Fig. 1. Here, an individual map period (or span) of length L is composed of N different fiber types, possibly interleaved with lumped amplifiers. The DM link is the repetition of N_s identical periods. Figure 1 shows a possible power gain profile within a period. The kth fiber of the span has length L_k, attenuation length $L_{Ak} \triangleq 1/\alpha_k$, average dispersion length L_{Dk}, average slope length L_{Dk}', and differential dispersion and slope lengths $L_{\Delta k}, L_{\Delta k}'$, respectively.

The gain profile inside the kth fiber, $k = 1,\dots,N$, of a generic period is

$$f(\zeta) = f(\zeta_k)\exp[-(\zeta-\zeta_k)/L_{Ak}], \qquad \zeta_k \leqslant \zeta < \zeta_{k+1},$$

where ζ is the local coordinate of the generic period; $\zeta_k = \Sigma_{n=1}^{k-1}L_n$ is the starting coordinate of the kth fiber, with $\zeta_1 = 0$; and $f(\zeta_k) = \Pi_{n=1}^{k-1}G_n\exp(-L_n/L_{An})$, with G_n as the gain of the lumped amplifier placed at $\zeta = \zeta_n$, and by the periodicity assumption $f(\zeta_1) = f(L) = 1$. The cumulated dispersion and slope phase rotations from $\zeta = 0$ to $\zeta = \zeta_k$ are accounted for in $\Theta_\Delta(\zeta_k,\omega)$, which can be expressed as
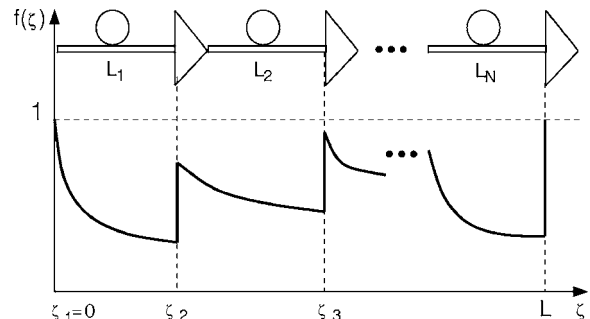
Fig. 1.   Power gain profile $f(\zeta)$ within a single period of a general periodic DM link. The overall link is the repetition of N_s periods.

$$\Theta_\Delta(\zeta_k,\omega) = \sum_{n=1}^{k-1}\left(\frac{\omega^2}{L_{\Delta n}} + \frac{\omega^3}{3L'_{\Delta n}}\right)L_n,$$

with $\Theta_\Delta(\zeta_1,\omega)=0$. Note that by periodicity also $\Theta_\Delta(L,\omega) = 0$ at the end of the period. We now have all the ingredients for evaluating the kernel $\mathcal{R}$ in expression (8), with the result

$$\mathcal{R}(\omega)z = \sum_{k=1}^{N} e^{j\Theta_\Delta(\zeta_k,\omega)}H_k(L_k,\omega), \qquad (21)$$

where $z=N_sL$ is the DM link length, and we introduce the filter $H_k(x,\omega)$ that weights the effects of the fast dynamics in the kth fiber:

$$H_k(x,\omega) = \Phi_{\mathrm{NL}k}\frac{L_{Ak}}{L_k^{\mathrm{eff}}}\frac{1 - \exp\left(-\dfrac{x}{L_{Ak}} + j\omega^2\dfrac{x}{L_{\Delta x}} + j\dfrac{\omega^3}{3}\dfrac{x}{L'_{\Delta k}}\right)}{1 - j\omega^2\dfrac{L_{Ak}}{L_{\Delta k}} - j\dfrac{\omega^3}{3}\dfrac{L_{Ak}}{L'_{\Delta k}}},$$

$$(22)$$

where $L_k^{\mathrm{eff}}=L_{Ak}[1-\exp-(L_k/L_{Ak})]$ is the effective nonlinear length of the kth fiber in the period and $\Phi_{\mathrm{NL}k}\triangleq N_s(L_k^{\mathrm{eff}}/L_{\mathrm{NL}k})f(\zeta_k)$ is the nonlinear phase cumulated within the N_s fibers of type k of the DM link.

Note that the above model also includes the case in which some fiber type has a negative distributed loss factor $\alpha_k = 1/L_{Ak}$; i.e., it has distributed gain, as in the case of lumped Raman amplification in the last fiber section of the period.

From now on, we will deal with the zero-dispersion slope case, except for Section 5 in which we will show that slope has indeed a negligible impact on PG in practical DM single-channel systems, unless the local dispersion is close to zero. In the absence of fiber dispersion slope, the operator $\mathcal{L}=\mathcal{L}_p$ is real ($\mathcal{L}_q=0$), as well as the operators $\mathcal{R}_p$ and $\mathcal{R}_q$, which thus represent the real and imaginary components of the kernel $\mathcal{R}$. Let us define the normalized kernel as $r(\omega)\triangleq\mathcal{R}(\omega)/\mathcal{R}(0)$, so that $\mathcal{R}(\omega)z=\Phi_{\mathrm{NL}}r(\omega)$. From Eq. (14) the eigenvalue thus becomes

$$kz = \Phi_{\mathrm{NL}}\sqrt{|r(\omega)|^2 - \left[1 - \mathrm{sgn}(\xi_{\mathrm{in}})\left(\frac{\omega}{\omega_c}\right)^2\right]^2}, \qquad (23)$$

where the critical frequency is defined as $\omega_c\triangleq\sqrt{2\Phi_{\mathrm{NL}}/|\xi_{\mathrm{in}}|}=\sqrt{2|L_D|/L_{\mathrm{NL}}}$ and is thus $\sqrt{2}$ times the soliton order.[1] Let k_r, k_i be the real and imaginary components of k. There are two possibilities: either (a) $k=k_r \ge 0$ and $k_i=0$, a condition that leads to modulation instability (MI) of the noise for increasing z,[1] or (b) $k=jk_i$, $k_i \ge 0$, and $k_r=0$, a condition of the absence of MI, which leads to a limited ASE PSD for increasing z. Since

$$|\mathcal{R}z| = \left|\int_0^L \frac{f(x)e^{j\Theta_\Delta(x,\omega)}}{L_{\mathrm{NL}}(x)}\mathrm{d}x\right| \le \int_0^L \frac{f(x)}{L_{\mathrm{NL}}(x)}\mathrm{d}x = \Phi_{\mathrm{NL}},$$

then $|r(\omega)|^2 \le 1$ for all ω, the equality holding at $\omega=0$. Thus by inspection of Eq. (23), one concludes that, for any DM scheme, MI can appear only with anomalous in-line dispersion, $\xi_{\mathrm{in}}>0$, at frequencies satisfying the following MI condition:

$$|r(\omega)| \ge \left|1 - \left(\frac{\omega}{\omega_c}\right)^2\right|. \qquad (24)$$

The fact that $\xi_{\mathrm{in}}\le 0$ ensures absence of MI was already proven for a symmetric lossless two-section map using Floquet theory.[24]

A. Map Strength

To compare different DM systems having different kernels, it is useful to expand the normalized kernel in a Taylor series around $\omega=0$. From the Taylor expansion of the exponential term in expression (8), we get

$$r(\omega) = \sum_{n=0}^{\infty}\frac{(-j)^n S_n}{n!}\omega^{2n} = 1 - jS_1\omega^2 - \frac{1}{2}S_2\omega^4 + j\frac{1}{6}S_3\omega^6 - \cdots,$$

$$(25)$$

where the nth-order DM strength is defined as

$$S_n \triangleq \left\langle\frac{f(z)}{L_{\mathrm{NL}}(z)}\left[\int_0^z\frac{\mathrm{d}x}{-L_\Delta(x)}\right]^n\right\rangle \Big/ \left\langle\frac{f(z)}{L_{\mathrm{NL}}(z)}\right\rangle. \qquad (26)$$

The frequency range over which the Taylor expansion [Eq. (25)] is accurate increases as we add higher-order terms. Suppose now the first-order strength S_1 term is dominant. When $|S_1|\omega^2 \ll 1$, i.e., when $\omega \ll \omega_\Delta \triangleq 1/\sqrt{|S_1|}$, then $r(\omega)\cong 1-jS_1\omega^2$ is a good approximation of the true kernel [Eq. (25)].

For our general kernel [Eq. (21)], a Taylor expansion to second order in ω of its main term gives

$$H_k(L_k,\omega) \cong \Phi_{\mathrm{NL}k}\left[1 + j\omega^2\frac{L_{Ak}}{L_{\Delta k}}\left(1 - \frac{L_k}{L_k^{\mathrm{eff}}}e^{-L_k/L_{Ak}}\right)\right],$$

so that from the Taylor expansion of $r(\omega)=\mathcal{R}(\omega)z/\Phi_{\mathrm{NL}}$ one finds

$$S_1 = -\sum_{k=1}^{N}\eta_k\left[\sum_{n=1}^{k-1}\frac{L_n}{L_{\Delta n}} + \frac{L_{Ak}}{L_{\Delta k}}\left(1 - \frac{L_k}{L_k^{\mathrm{eff}}}e^{-L_k/L_{Ak}}\right)\right], \qquad (27)$$

which shows that the contribution of each fiber type in the span to the (first-order) strength scales with the fraction of nonlinear phase in that type

$$\eta_k \triangleq \frac{\Phi_{\mathrm{NL}k}}{\Phi_{\mathrm{NL}}} = \frac{\dfrac{L_k^{\mathrm{eff}}}{L_{\mathrm{NL}k}}f(\zeta_k)}{\displaystyle\sum_{n=1}^{N}\frac{L_n^{\mathrm{eff}}}{L_{\mathrm{NL}n}}f(\zeta_n)},$$

with $\Sigma_{k=1}^{N}\eta_k=1$. The periodicity constraint $\Theta_\Delta(L,\omega)=0$ translates here into the constraint

$$\sum_{n=1}^{N}\frac{L_n}{L_{\Delta n}} = 0. \qquad (28)$$

We will see the importance of the strength S_1 as we proceed to the numerical evaluation of specific kernels.

B. General Power Spectral Densities

In the absence of slope, the normalized ASE PSDs [Eqs. (19)] become explicitly

$$\hat{S}_{pp}(\omega) = c_0(\omega) + [c_2(\omega)r_r(\omega) - c_1(\omega)r_i(\omega)],$$

$$S_{qq}(\omega) = c_0(\omega) + [c_2(\omega)r_r(\omega) - c_1(\omega)r_i(\omega)],$$

$$S_{pq}(\omega) = -[c_1(\omega)r_r(\omega) + c_2(\omega)r_i(\omega)],\qquad(29)$$

with real coefficients:

$$c_0 = f_1 + f_2[\Phi_{NL}^2|r|^2 + (\mathcal{L}_p z)^2]$$

$$= 1 + \Phi_{NL}^2|r|^2\left[\frac{\sinh(2kz)}{2kz} - 1\right]\Big/ (kz)^2,$$

$$c_1 = 2\Phi_{NL}f_3 = 2\Phi_{NL}[\cosh(2kz) - 1]/(2kz)^2,$$

$$c_2 = 2\Phi_{NL}f_2\mathcal{L}_p z = \Phi_{NL}^2\left[1 - \mathrm{sgn}(\xi_{in})\left(\frac{\omega}{\omega_c}\right)^2\right]$$

$$\times\left[\frac{\sinh(2kz)}{2kz} - 1\right]\Big/ (kz)^2,\qquad(30)$$

with kz given in Eq. (23). Note that c_0 is half the physically observable normalized PSD $\hat{S}_{pp}+\hat{S}_{qq}$ of the overall ASE process, commonly referred to as MI spectral gain.[10,12] From the above formulas, it is clear that PG for any kernel scales with the following three dimensionless key parameters: (1) nonlinear phase Φ_{NL} (rad); (2) normalized total in-line dispersion ξ_{in} (through kz and ω_c); and (3) map strength S_1 that determines the kernel r when $\omega \ll \omega_\Delta$. Higher-order strengths are required to uniquely determine PG over a larger frequency range.

4. SOME KERNELS OF INTEREST
We now specialize the theory in Section 2 to several periodic DM links of interest, which can all be described as special cases of the general case shown in Fig. 1.

A. Long-Span Terrestrial Link
Each map period in a standard terrestrial DM link is composed of $N=2$ fiber types: a transmission fiber of length much longer than its attenuation length, which is followed by a dispersion-compensating fiber (DCF). If the DCF is ideal, i.e., no nonlinearity is present in the DCF (e.g., a grating[11] or a DCF with low input power), then

$$\mathcal{R}z \cong H_T(L_T, \omega) = \frac{\Phi_{NL}}{1 + jS\omega^2},\qquad(31)$$

where subscript T refers to the transmission fiber, and we define $S = -L_{AT}/L_{\Delta T}$ as the map strength of the long-span terrestrial system. S has the sign of the dispersion coefficient D_T [ps/(nm km)] and is, in fact, the first-order strength as defined in expression (26). A graphical representation of the functions of ω on both sides of expression (24) is plotted in Fig. 2 versus normalized frequency $f_n \triangleq \omega/2\pi$, where the monotonically decreasing kernel modulus is shown for various strength values. In the absence of DM ($S=0$) and at positive in-line $\xi_{in} > 0$, we see that MI is confined to the range $0 < \omega \leq \sqrt{2}\omega_c$. As compared with the non-DM case, at the same Φ_{NL} and in-line ξ_{in}, we
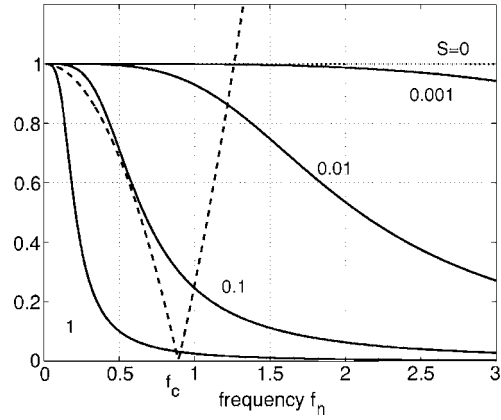
Fig. 2.   Plot of $|r|$ (solid curves) and $|1-(\omega/\omega_c)^2|$ (dashed curve) versus normalized frequency $f_n = \omega/2\pi$, at $\Phi_{NL}=0.5\pi$ and $\xi_{in}=0.1$. Critical frequency $f_c \triangleq \omega_c/2\pi$.

note that DM shrinks the frequency range over which MI appears by an increasing amount as the strength S increases and independently of the sign of S. At small $|S|$, only one root $\omega_c < \omega_1 < \sqrt{2}\omega_c$ of expression (24) is present, while at a critical strength (here $|S|=0.1$) tangency between the right and the left functions in expression (24) is reached, so that at larger strengths two more roots ω_2 and ω_3 appear (we assume $\omega_1 < \omega_2 < \omega_3$) so that MI is confined to the range $\omega \in [0,\omega_1] \cup [\omega_2,\omega_3]$. At large $|S|$ the interval $[\omega_2,\omega_3]$ shrinks around ω_c.

In the following we verify the accuracy of our theoretical asymptotic PG formulas (29) against direct solution of the linearized propagation equation with ASE using the split-step Fourier method[1] (SSFM).

1. Case $S=0$
We start with the simplest case of an uncompensated system, in which the local dispersion matches the average dispersion and thus $S=0$.

Figure 3 shows the normalized ASE PSDs versus normalized frequency f_n in a system with $S=0$ and $\Phi_{NL}=0.5\pi$ rad. SSFM simulations (solid curves) have been performed for $N_s=5,10,15,50$ spans. The top row shows the PSDs $\hat{S}_{qq}$ and $\hat{S}_{pp}$ on a decibel scale, while the bottom row shows $\hat{S}_{pq}$ on a linear scale. The left column refers to a normal transmission fiber with $\xi_{in}=-0.1275$, while the right column reports the same quantities in the anomalous case $\xi_{in}=0.1275$. To appreciate the meaning of the normalized quantities in the figure, for instance, for a reference nonreturn-to-zero (NRZ) signal at 10 Gb/s, the normalized frequency $f_n=1$ corresponds to 10 GHz, while $\xi_{in}=0.1275$ corresponds to an in-line cumulated dispersion of ±1000 ps/nm at $\lambda=1550$ nm. In all figures, dashed curves correspond to our asymptotic formulas (29). We note the well-known features of the inflation of $\hat{S}_{pp}$ above its linear value of 1 in the anomalous regime and its deflation below 1 in the normal regime (noise squeezing).[7] In the figures, we also see that the SSFM-simulated ASE PSDs converge to the theoretical asymptotic formulas (29) for increasing N_s, which becomes practically indistinguishable from simulations beyond $N_s=50$. However, we see that already at $N_s=10$ spans the prediction is less than 0.7 dB on the whole frequency range. The

formulas represent a lower bound (at most frequencies) of the simulated PSDs for finite spans, which in the present case includes a booster with the same noise figure as the line amplifiers. We verified that without such a booster the formula yields an upper bound on the simulated PSDs.

We also note that at a small number of spans ($N_s=5$) there are significant sideband instability (SI) lobes, which disappear at larger N_s. This is fortunate, since the averaged NLSE is able to reproduce only the main lobe of MI, while SI lobes are captured only when the higher harmonics in the Fourier expansion of the periodic NLSE parameters are also taken into consideration.[9]

Note that when $S=0$ we have $r(\omega)=1$, and we already noted that MI is present in the range $0<\omega<\sqrt{2}\omega_c$. Using

$r_r=1$ and $r_i=0$ in Eqs. (29), it is easy to see that $\hat{S}_{pp}$ and $\hat{S}_{qq}$ cross only when $\xi_{in}>0$, and such a crossing occurs at $\omega=\omega_c$. Also, since $kz\to0$ as $\omega\to\sqrt{2}\omega_c$, then from Eqs. (29) we find that for all $\xi_{in}>0$: (i) $\hat{S}_{qq}(\sqrt{2}\omega_c)=1$, which provides a simple way of spotting out from the plot of the quadrature PSD the value of $\sqrt{2}\omega_c$, which is also an estimate of the width of the main lobe of $\hat{S}_{qq}$; (ii) $\hat{S}_{pp}(\sqrt{2}\omega_c)=1+\frac{4}{3}\Phi_{NL}^2$, which equals the value of $\hat{S}_{qq}$ at $\omega=0$ and is close to the actual peak value; and (iii) $\hat{S}_{pq}(\sqrt{2}\omega_c)=-\Phi_{NL}$.

2. Case $\xi_{in}=0$
We now tackle the special case of a terrestrial DM system with full in-line compensation, $\xi_{in}=0$. Figure 4 shows the
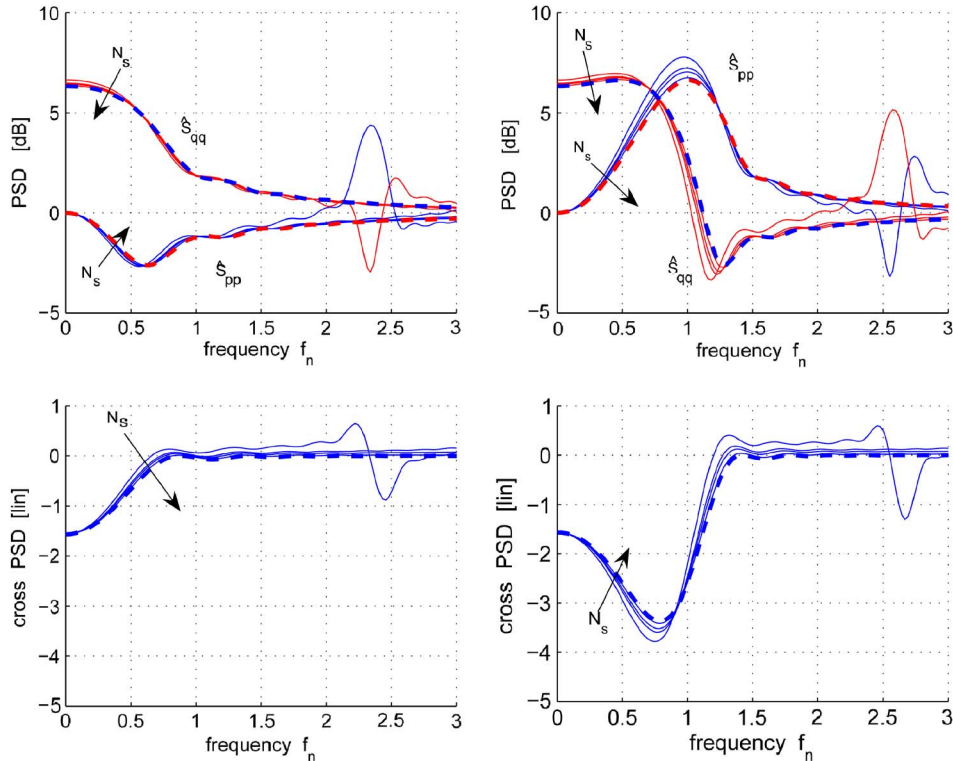
Fig. 3. (Color online) Normalized ASE PSDs (top: $\hat{S}_{pp}$ and $\hat{S}_{qq}$; bottom: $\hat{S}_{pq}$) versus normalized frequency f_n in an uncompensated system ($S=0$) with $\Phi_{NL}=0.5\pi$, and $\xi_{in}=-0.1275$ (left), $\xi_{in}=0.1275$ (right). Solid curves: SSFM simulations for $N_s=5,10,15,50$. Dashed curves: theory [Eqs. (29)].
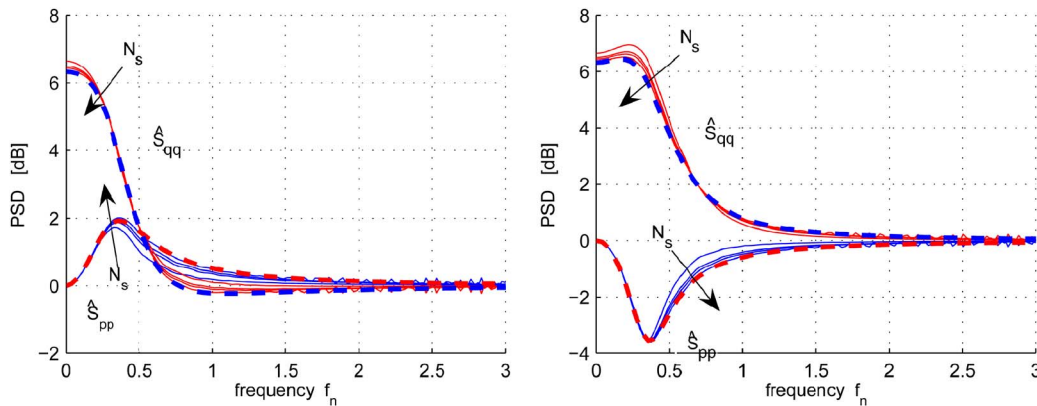
Fig. 4. (Color online) Normalized ASE PSDs versus normalized frequency f_n in a DM system with full in-line compensation, with $\Phi_{NL}=0.5\pi$, $S=-0.1275$ (left), and $S=0.1275$ (right). Solid curves: SSFM simulations for $N_s=5,10,15,50$. Dashed curves: theory [Eqs. (29)].

normalized ASE PSDs versus frequency f_n, for $S = -0.1275$ (left column), $S = 0.1275$ (right column), and $\Phi_{NL} = 0.5\pi$ rad. The strength can be expressed in terms of physical parameters as

$$S = \frac{\chi}{\alpha}\left(D_T - \frac{D_n}{N_s L}\right), \tag{32}$$

where $\chi \triangleq (1/2\pi c)(\lambda/T)^2$, c is the light speed, $D_{in} = \xi_{in}/\chi^-$ (usually expressed in ps/nm) is the overall in-line cumulated dispersion, while D_T is the transmission fiber dispersion coefficient [usually in ps/(nm km)]. Hence $S = 0.1275$ could be, for instance, the map strength of an NRZ system at $R = 40$ Gb/s at $\lambda = 1550$ nm, with a nonzero dispersion-shifted (NZDSF$^+$) transmission fiber [$D_T = 2.92$ ps/(nm km)]. Comparing Fig. 4 with Fig. 3, we note that both $\hat{S}_{pp}$ and $\hat{S}_{qq}$ are much less inflated by PG in both the anomalous and the normal regimes. In the figures we see both theory [Eqs. (29)] (dashed curves) and SSFM simulations (solid curves) for increasing number of spans $N_s = 5, 10, 15, 50$, and we note a quick convergence to the theory for increasing N_s. Already at five spans the prediction is within 1 dB of the actual value over the whole frequency range. Using expression (31), Eqs. (29) become explicitly

$$\hat{S}_{pp} = 1 - \frac{1 - \cos\nu}{2\Phi_{NL}S\omega^2},$$

$$\hat{S}_{qq} = 1 + \frac{1 - \cos\nu}{2\Phi_{NL}S\omega^2} + \frac{2}{S^2\omega^A}\left(1 - \frac{\sin\nu}{\nu}\right),$$

$$\hat{S}_{pq} = -\frac{1 - \cos\nu}{2\Phi_{NL}S^2\omega^4} + \frac{1}{S\omega^2}\left(1 - \frac{\sin\nu}{\nu}\right), \tag{33}$$

where $\nu \triangleq -2\Phi_{NL}S\omega^2/\sqrt{1 + S^2\omega^4}$. Thus we easily see that $\hat{S}_{pp}$ is always inflated (above 1) for normal transmission fiber ($S < 0$) and deflated for anomalous fiber. However, even in the normal case we have that an upper bound on $\hat{S}_{pp}$ is $1 - 1/(\Phi_{NL}S\omega^2)$. Hence the in-phase component does not diverge for increasing nonlinear phase, since systems with full in-line compensation do not display MI, as already noted in Section 3. Note that $|\nu|$ varies from 0 to $2\Phi_{NL}$ as ω increases. The frequency ω at which the midvalue $|\nu| = \Phi_{NL}$ is reached is obtained by solving the equation $1 = 4S^2\omega^4/(1 + S^2\omega^4)$ and turns out to be $\bar{\omega} = \omega_\Delta/\sqrt[4]{3} \cong 0.76\omega_\Delta$, with ω_Δ defined in Subsection 3.A. We note that $\bar{\omega}$ is also close to the maximum (if $S < 0$) or minimum (if $S > 0$) of $\hat{S}_{pp}$. The width of the main lobe of the function $2c_0 \triangleq \hat{S}_{pp} + \hat{S}_{qq}$, i.e., the PSD of the ASE process $a(z,t)$, can be taken as an estimate of the range over which PG inflates the PSDs. We define the PG bandwidth ω_{PG} as that frequency at which $c_0(\omega_{PG}) = [c_0(0) + c_0(\infty)]/2$, i.e., is halfway between $c_0(0) = 1 + \frac{2}{3}\Phi_{NL}^2$ [from Eq. (20)] and $c_0(\infty) = 1$. We search ω_{PG} in the neighborhood of $\omega = 0$, so that, by approximating $f_{1,2}$ with their fourth-order Taylor expansion around $kz = 0$, we find

$$\omega_{PG} \cong \left(\frac{\sqrt{\Phi_{NL}^4 + 25} - \Phi_{NL}^2}{5}\right)\omega_\Delta, \tag{34}$$

according to which ω_{PG} decreases for increasing Φ_{NL}. Such a formula has been verified to be accurate to within 5% of the true value in the range $0 < \Phi_{NL} < \pi$.

3. Case $\xi_{in} \neq 0$, $S \neq 0$

We consider three sample DM long-span terrestrial systems. Type 1 has single-mode (SMF) transmission fiber [$D_T = 17$ ps/(nm km) at 1550 nm], type 2 is NZDSF$^+$ [$D_T = 2.92$ ps/(nm km)], and type 3 is NZDSF$^-$ [$D_T = -2.60$ ps/(nm km)], all with attenuation $\alpha = 0.2$ dB/km. Referred to an NRZ 10 Gb/s transmission, in the limit of $N_s \to \infty$ and for a finite in-line dispersion, from Eq. (32) the three systems have strenghts $S = 0.0485, 0.0095, -0.0058$, respectively. We now compare links of different number of spans, at fixed nonlinear phase, strength, and in-line dispersion.

Figure 5 shows the in-phase and quadrature ASE PSDs for all three types of fiber according to our asymptotic formula [Eqs. (29)] (dashed curves) and the SSFM-simulated curves (solid curves) for $N_s = 5, 10, 15, 50$ spans, all at the same nonlinear phase $\Phi_{NL} = 0.72\pi$ and $\xi_{in} = 0.1275$. Again, we note that at five spans there are some contributions due to SI, which disappear for increasing N_s. Complete convergence to our formula is achieved roughly around $N_s \cong 50$. Hence the main system parameter to ensure convergence is the nonlinear phase rotation per span, which should be smaller than 0.1 rad, although the convergence speed slightly depends also on the details of the map. A theoretical investigation of convergence of the DM-NLSE can be found in Ablowitz *et al.*[25] Note also that a closed-form expression for the PSDs for any N_s is known,[11] which matches the simulated PSD curves in the main PG
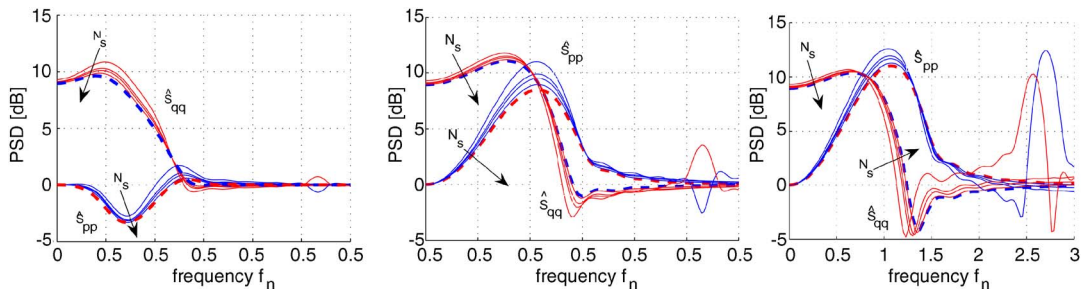
Fig. 5. (Color online) Normalized ASE PSD $\hat{S}_{pp}$ and $\hat{S}_{qq}$ versus frequency f_n, in a DM system with $\xi_{in} = 0.1275$ (1000 ps/nm at 10 Gb/s) and with $\Phi_{NL} = 0.72\pi$ rad for the (left) SMF system ($S = 0.0485$); (center) NZDSF$^+$ system ($S = 0.0095$); (right) NZDSF$^-$ system ($S = -0.0058$). Solid curves: SSFM simulations for $N_s = 5, 10, 15, 50$. Dashed curves: theory [Eqs. (29)].
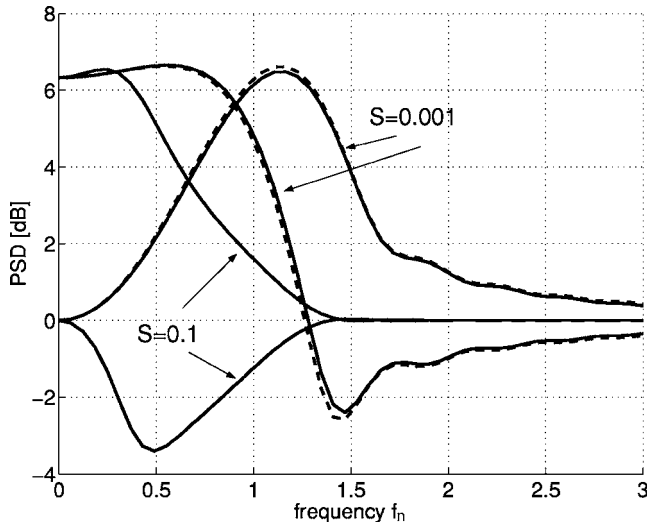
Fig. 6. (solid curves) ASE PSDs versus frequency for a long-span terrestrial link with $\Phi_{\text{NL}}=0.5\pi$, $\xi_{\text{in}}=0.1$, and both $S=0.1$ and $S=0.001$. (dashed curves) $S=0$ unmapped case.

lobe but does not capture the SI, since such a formula is also based on an averaged NLSE.

From comparison of the two NZDSF plots in Fig. 5, one concludes that the sign of the transmission fiber dispersion does not significantly affect the shape of the PSDs. This is confirmed by the MI condition (24), whose solutions depend on strength S only through $|r|$ and thus are independent of the sign of S. A related interesting observation was made in Ciaramella and Tamburrini[12] regarding the discrepancy of the PSDs between an unmapped link ($S=0$) and a DM link operated at the same Φ_{NL} and ξ_{in}. It was noted that at large in-line dispersion ξ_{in} the strength does not contribute to setting the PSDs. However, how large an in-line dispersion is required was quantified only in the special case of an SMF-based link.[12] We are now able to generalize that result. From Fig. 2, one may guess that if the graph of the curve $|1-(\omega/\omega_c)^2|$ intercepts the graph of $|r(\omega,S)|$ at a frequency ω close to $\sqrt{2}\omega_c$, then the behavior of the eigenvalue kz, and thus of the PSDs, should be similar to the unmapped case. This requires that the kernel near the intercept frequency $\sqrt{2}\omega_c$ be described by $r\cong 1-jS\omega^2$, with $|S|\omega^2\ll 1$. Hence no significant difference in PSDs between the mapped and the unmapped cases is expected when

$$|\xi_{\text{in}}| \geqslant 4\Phi_{\text{NL}}|S|. \tag{35}$$

Using the same system values as in Fig. 2, we show in solid curves in Fig. 6 the in-phase (concave curves) and quadrature (convex curves) ASE PSDs at $S=0.1$ and $S=0.001$, while the unmapped case is shown in dashed curves. The largest strength does not satisfy expression (35), although the smaller one does. Condition (35) holds in fact for any kernel, by using the first-order strength introduced in Subsection 3.A.

B. General Terrestrial Link
Consider again a terrestrial DM link, with $N=2$ fiber types per span, but now we account for nonlinearity in the DCF and for the possibility that the transmission–DCF fi-

bers may be of length comparable with their attenuation length. From Eq. (21), the kernel explicitly is

$$\mathcal{R}z = H_T(L_T,\omega) + e^{j\omega^2 L_T/L_{\Delta T}}H_C(L_C,\omega), \tag{36}$$

where we used subscript T for the transmission fiber and C for the compensating one.

Figure 7 (left) shows normalized ASE PSDs versus frequency f_n with a cumulated in-line dispersion $\xi_{\text{in}}=-0.025$ (−200 ps/nm at $R=10$ Gb/s). Symbols denote SSFM simulations for $N_s=20$ spans, each span being composed of L_T km of transmission fiber [$D_T=8$ ps/(nm km), $\alpha_T=0.2$ dB/km, $\gamma_T=2$ W^{-1} km^{-1}], L_T being 10, 50, or 100 km, followed by a DCF [$D_C=-100$ ps/(nm km), $\alpha_C=0.6$ dB/km, $\gamma_C=6$ W^{-1} km^{-1}], and with a single amplifier at the end of the DCF to recover the span losses. The non-linear phase was $\Phi_{\text{NL}}=0.72\pi$ rad in all three length cases.[26] Solid curves denote theory [Eqs. (29)], making use of Eq. (36), and well agree with simulations. We note that shortening the transmission fiber length from 100 to 10 km implies increasing the fraction of nonlinear phase inside the DCF. This has the effect of significantly shifting the dip of the in-phase PSD to higher frequencies, as in an equivalent long-span terrestrial system (a terrestrial system with transmission fiber much longer than its attenuation length and no nonlinearity in DCF, as in Subsection 4.A) with smaller transmission fiber dispersion, as shown in Fig. 7 (right), where the best fit of the PSDs in the $L_T=10$ km case was found at an equivalent transmission fiber dispersion of $D_{\text{eq}}=1.9$ ps/(nm km).

For the same system with $D_T=8$ ps/(nm km) and $L_T=100$ km of Fig. 7, Fig. 8 (left) shows the effect of using the DCF within a dual-stage amplifier, with relative power into the DCF $P_{\text{DCF}}/P=0,-3,-20$ dB, the third value corresponding to the previous case of the absence of the first amplifier. The PSDs were derived by using Eqs. (29) and (36). We note that the effect of increasing the power (and thus the nonlinear effect) into the DCF is that of shifting the dip of the in-phase PSD to lower frequencies, as in an equivalent long-span system with smaller transmission fiber dispersion, as shown in Fig. 8 (right), where the best fit of the PSDs in the $P_{\text{DCF}}/P=0$ dB case was found at an equivalent fiber dispersion $D_{\text{eq}}=12.8$ ps/(nm km).

The explanation of the above-observed equivalence of PSDs is rooted in the concept of map strength. In both previous cases the fraction of nonlinear phase into the DCF is

$$\eta_c = \gamma_C L_C^{\text{eff}}\frac{P_{\text{DCF}}}{P} \left/ \left(\gamma_T L_T^{\text{eff}} + \gamma_C L_C^{\text{eff}}\frac{P_{\text{DCF}}}{P}\right)\right.,$$

where the ratio P_{DCF}/P reaches its lowest value $e^{-L_T/L_{AT}}$ in the absence of the amplifier preceding the DCF. Define the strength of the transmission fiber as $S_T\triangleq-L_{AT}/L_{\Delta T}$, and define S_C similarly for the DCF. Then constraint (28) here gives $S_C=-S_T(L_T/L_{AT})(L_{AC}/L_C)$. Thus Eq. (27) finally gives the equivalent (first-order) strength of the terrestrial DM link as
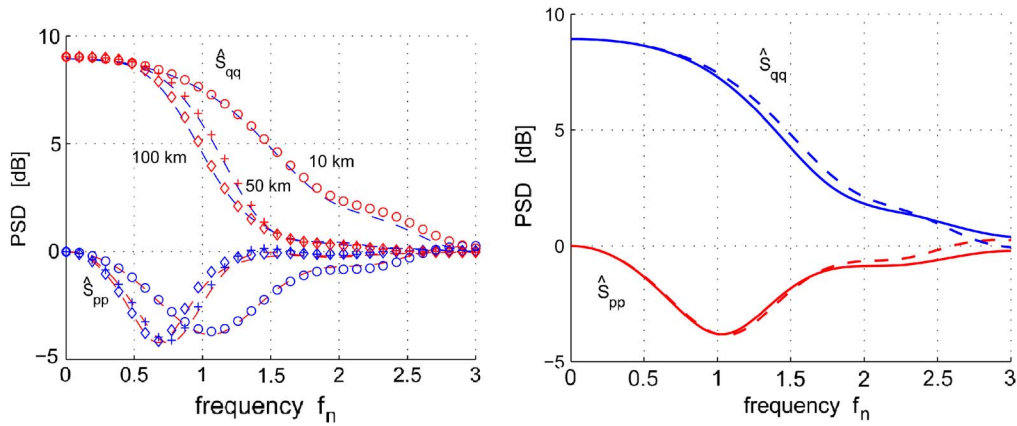
Fig. 7.   (Color online) Normalized ASE PSD $\hat{S}_{pp}$ and $\hat{S}_{qq}$ versus frequency f_n at $\Phi_{NL}=0.72\pi$ rad and cumulated in-line dispersion $\xi_{in}=-0.025$ (-200 ps/nm at $R=10$ Gb/s). Left: theory [Eqs. (29)] (dashed curves) and SSFM simulations (symbols) for 20-span terrestrial map with $D_T=8$ ps/(nm km), $D_C=-100$ ps/(nm km), and various lengths $L_T=10,50, 100$ km. Right: PSDs for $L_T=10$ km case as in left plot (dashed curves) and equivalent long-span system with $D_{eq}=1.9$ ps/(nm km) (solid curves).
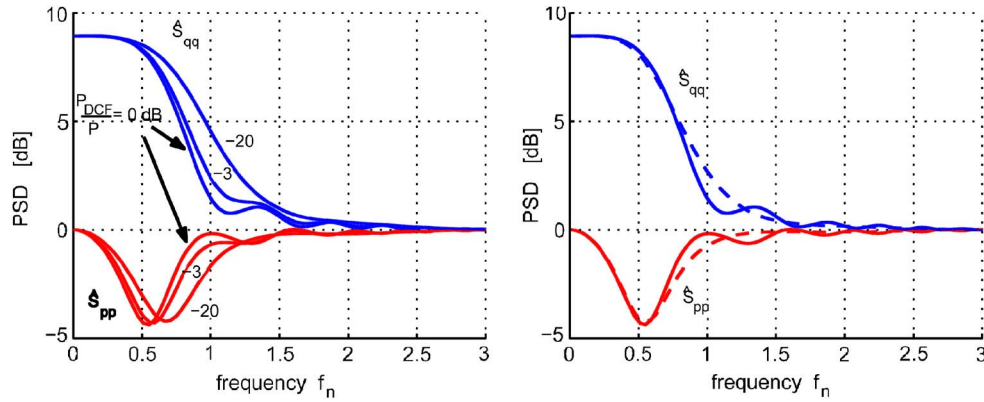
Fig. 8.   (Color online) Normalized ASE PSD $\hat{S}_{pp}$ and $\hat{S}_{qq}$ versus frequency f_n, in a system with $\Phi_{NL}=0.72\pi$ rad, $\xi_{in}=-0.025$, and terrestrial map with $L_T=100$ km. Left: two-section span with DCF within dual-stage amplifier, with $D_T=8$ ps/(nm km), $D_C=-100$ ps/(nm km), and various ratios $P_{DCF}/P=-20$, -3, 0 dB. Right: PSDs for the $P_{DCF}/P=0$ dB case as in left figure (solid curves) and equivalent long-span system (dashed curves) with $D_{eq}=12.8$ ps/(nm km).

$$S_1 = S_T \left\{ (1 - \eta_c) \left(1 - \frac{L_T}{L_T^{eff}} e^{-L_T/L_{AT}} \right) \right.$$
$$\left. + \eta_c \frac{L_T}{L_{AT}} \left[1 - \frac{L_{AC}}{L_C} \left(1 - \frac{L_C}{L_C^{eff}} e^{-L_C/L_{AC}} \right) \right] \right\}. \quad (37)$$

It was, in fact, using Eq. (37) that the strength of the best-matching equivalent long-span system was found in Figs. 7 and 8. Also note that the largest frequency for an acceptable PSD matching extends roughly up to $\omega_\Delta = 1/\sqrt{|S_1|}$.

We show in Fig. 9 S_1/S_T versus L_T obtained from Eq. (37) for different values of η_c, having used the same attenuation and dispersion values as in Fig. 7. We note that for a fixed L_T the first-order map strength increases with the nonlinear phase cumulated in the DCF. If both types of fiber are significantly longer than their attenuation lengths, Eq. (37) simplifies to $S_1 \cong S_T[(1 - \eta_c) + \eta_c(L_T/L_{AT})]$. For example, for typical 100 km terrestrial spans with standard transmission fiber, one has $L_T/L_{AT} \cong 5$. Hence if 75% of the nonlinearity takes place in the transmission fiber and 25% in the DCF, the first-order
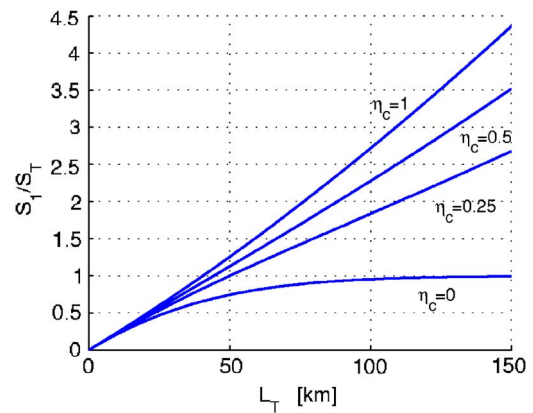
Fig. 9.   (Color online) S_1/S_T versus transmission fiber length L_T for varying η_c. Same attenuation and dispersion values as in Fig. 7.

map strength S_1 is increased from S_T by a factor $0.75 + 0.25(5)=2$, as can be checked in Fig. 9.

C. Submarine Link
We consider a typical submarine map, whose period is composed of $L_1=l$ km of a fiber with dispersion $+D$, fol-

lowed by $L_2 = 2(l - \epsilon)$ km of a fiber with the same parameters but opposite dispersion $-D$ and by a third fiber equal to the first one.[17] All fibers have the same attenuation length L_A, and amplification is provided only at the end of each period. The parameter ϵ sets the desired amount of residual dispersion per span, and $\epsilon \ll l$ for many-span links. Applying Eq. (21) and again neglecting the fiber's slope give $\mathcal{R}z = (1 + e^{-3l/L_A - j\omega^2 l/L_{\Delta 1}})\ H_1(l, \omega) + e^{j\omega^2 l/L_{\Delta 1}} H_2(2l, \omega)$ which after some algebra can be explicitly written as[17]

$$\mathcal{R}z = \Phi_{NL} \frac{1 + S\omega^2 \operatorname{csch}(G)\sin(SG\omega^2) - jS\omega^2[1 - \operatorname{sech}(G)\cos(SG\omega^2)]}{1 + S^2\omega^4}, \tag{38}$$

which is seen to depend on the two dimensionless parameters $S \triangleq -L_A/L_{\Delta 1}$ and $G \triangleq l/L_A$. As the fiber attenuation goes to zero, the kernel reduces to $\mathcal{R}z = \Phi_{NL}\sin(SG\omega^2)/(SG\omega^2)$, and all odd-index strengths $S_1, S_3, \ldots$, vanish.[11,17] The zero-loss case is extensively studied in the soliton literature, and thus the only parameter of the submarine lossless kernel $s \triangleq SG$ is called in that context the map strength.[17] In the lossy case, from the Taylor expansion of Eq. (38), the first two strengths [expression (26)] are found to be

$$S_1 = S[1 - \operatorname{sech}(G)],$$

$$S_2 = 2S^2[1 - G\operatorname{csch}(G)]. \tag{39}$$

The expression of S_1 could be obtained directly from Eq. (27). Although at low loss the term with S_2 dominates that with S_1, the first two terms of the kernel Taylor expansion have equal magnitude at $\omega = \omega_\Delta$ (as in a long-span terrestrial system) when $|S_1| = \sqrt{S_2/2}$, i.e., when $l/L_A \cong 1.2$. Therefore, when each fiber in the period is longer than its attenuation length, there exists an equivalent long-span terrestrial kernel with strength S_1 that well approximates the submarine kernel over the region $0 < \omega < \omega_\Delta$.

In Fig. 10 we show the PSDs for an alternating $+D$, $-D, +D$ three-section span with $l = 15$ km, $D = 8$ ps/(nm km), $\Phi_{NL} = 0.72\pi$ rad, along with their equivalent long-span fit whose equivalent transmission fiber dispersion $D_{eq} = D[1 - \operatorname{sech}(G)] \cong 1.6$ ps/(nm km) was obtained from Eqs. (39).

5. EFFECT OF SLOPE

The effect of dispersion slope on ASE PSDs is generally negligible, unless the local dispersion is close to zero, as, for instance, in dispersion-shifted fibers. Figure 11 shows the ASE PSDs [Eqs. (19)] for a fully compensated DM system with two-section spans, with 50 km at dispersion $+D$ and slope $+\mathcal{S}$, followed by 50 km at $-D$ and slope $-\mathcal{S}$, with $D = 0.1$ ps/(nm km) and $\mathcal{S} = 0.058$ ps/(nm² km), and with common fiber attenuation $\alpha = 0.2$ dB/km and amplification provided only at the end of the span, and for a nonlinear phase $\Phi_{NL} = 0.72\pi$ rad. The figure also shows in dashed curves the PSDs when dispersion slope is neglected. We note that in this case dispersion slope causes the growth of a second sidelobe at higher frequencies.

6. IMPACT OF POSTCOMPENSATION

Commonly installed optical systems make use of precompensating and postcompensating fibers, placed before and after the link, respectively, to improve the tolerance to linear and nonlinear distortions. While the precompensating fiber has no effect on PG, since ASE is generated downstream of it, in this section we investigate the effect of the postcompensating fiber (postfiber in brief) on PG.

Propagation inside the postfiber is still governed by the dynamical equation (5), yielding an input–output relation described by a transfer matrix $\mathbf{U}$. If nonlinearity and dispersion slope within the postfiber are neglected, matrix $\mathbf{U}$ is a real orthogonal (rotation) matrix, which can be obtained from Eq. (15) in the limit $\Phi_{NL} \to 0$ as $\mathbf{U} = [\cos\theta_p, -\sin\theta_p; \sin\theta_p, \cos\theta_p]$, with a post rotation angle $\theta_p = \xi_{post}\omega^2/2$, where ξ_{post} is the normalized cumulated dispersion in the postfiber. From expression (16) the received ASE PSD matrix after postcompensation is

$$\tilde{\mathbf{S}} = \mathbf{U}\hat{\mathbf{S}}\mathbf{U}^\dagger. \tag{40}$$
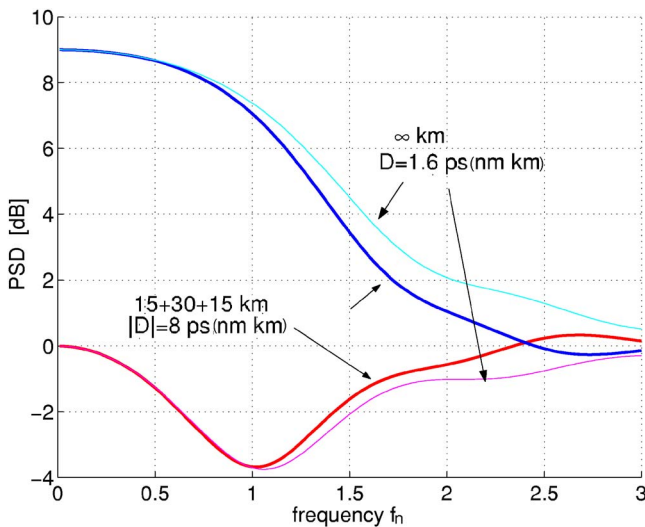
Fig. 10. (Color online) $\hat{S}_{pp}$ (concave) and $\hat{S}_{qq}$ (convex) versus frequency f_n for a three-section span with 15 km at dispersion $+D$, 30 km at $-D$, and 15 km at $+D$, and D is 8 ps/(nm km). $\Phi_{NL} = 0.72\pi$ rad. PSDs of equivalent long-span fit with $D_{eq} = 1.6$ ps/(nm km) also shown.
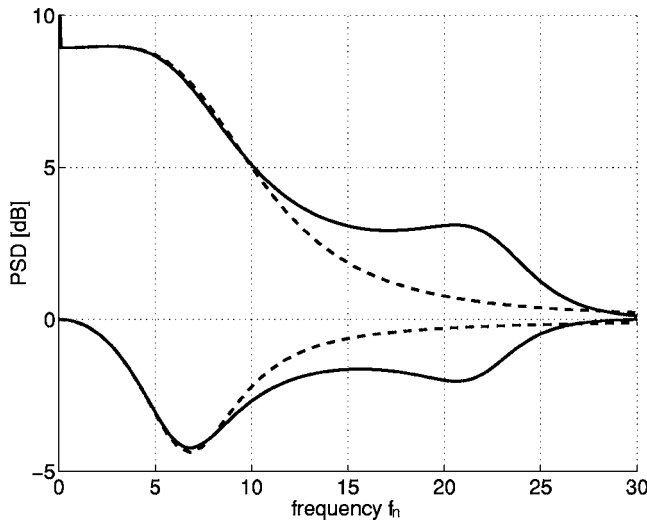
Fig. 11. $\hat{S}_{pp}$ (concave) and $\hat{S}_{qq}$ (convex) versus frequency f_n for a fully compensated two-section span with 50 km at dispersion $+D$ and slope $+\mathcal{S}$ and 50 km at $-D$ and slope $-\mathcal{S}$, with $D = 0.1$ ps/(nm km) and $\mathcal{S} = 0.058$ ps/(nm² km). PSDs ignoring dispersion slope are shown, as dashed curves. $\Phi_{NL} = 0.72\pi$ rad.
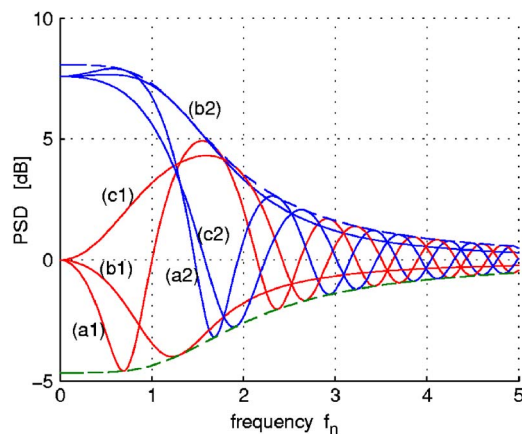
Fig. 12. (Color online) ASE PSD for different postcompensations. (a) $\xi_{post} = -0.025$; (b) $\xi_{post} = 0$; (c) $\xi_{post} = 0.025$. Index 1: in-phase component; index 2: quadrature component. Dashed curves: eigenvalues λ_m, λ_M. $S = 0.01$, $\xi_{in} = 0$, $\Phi_{NL} = 0.6\pi$.

As an example, in Fig. 12 the received ASE PSDs are plotted for different values of postcompensation $\xi_{post} = [-0.025, 0, 0.025]$ for a long-span terrestrial DM system having map strength $S = 0.01$, nonlinear phase $\Phi_{NL} = 0.6\pi$, and full in-line compensation $\xi_{in} = 0$. As can be observed, the behavior of the PSDs strongly depends on the amount of postcompensation, with a periodic exchange of power between the in-phase and quadrature components as the frequency increases.

To understand such a power transfer, it is useful to spectrally decompose the positive semidefinite PSD matrix as $\hat{\mathbf{S}} = \mathbf{V}\boldsymbol{\Lambda}\mathbf{V}^\dagger$, where $\boldsymbol{\Lambda} = \mathrm{diag}([\lambda_m, \lambda_M])$ is the diagonal matrix of its real nonnegative minimum and maximum eigenvalues, respectively, while the columns of the unitary matrix $\mathbf{V}$ are the corresponding orthonormal eigenvectors. If dispersion slope in the DM line is neglected, then the f_3 term in Eqs. (18) is real, and thus the diagonal term $\hat{S}_{pq}$ is also real. Hence $\mathbf{V}$ is a real rotation matrix,

which can be written as $\mathbf{V} = [\cos\hat{\theta}, -\sin\hat{\theta}; \sin\hat{\theta}, \cos\hat{\theta}]$. The line rotation angle $\hat{\theta}$ can be found from the spectral decomposition form to be

$$\hat{\theta}(\omega) = \frac{1}{2}\arctan\left(\frac{2\hat{S}_{pq}}{\hat{S}_{pp} - \hat{S}_{qq}}\right). \tag{41}$$

The eigenvalues are found to be $\lambda_{m,M} = \frac{1}{2}[\hat{S}_{pp} + \hat{S}_{qq} \pm \sqrt{(\hat{S}_{pp} - \hat{S}_{qq})^2 + 4\hat{S}_{pq}^2}]$, and, after using Eqs. (29), they simplify to $\lambda_{m,M} = c_0 \pm |r|\sqrt{c_1^2 + c_2^2}$, a relation that shows, for instance, that they do not depend on the sign of the strength S of the terrestrial kernel, since the strength always appears inside the term $|r|$. The similarity transformation [Eq. (40)] preserves the eigenvalues. Thus from the Rayleigh–Ritz theorem[27] we have $\lambda_m = \min_{\|\mathbf{x}\|=1}\mathbf{x}^T\widetilde{\mathbf{S}}\mathbf{x}$ and $\lambda_M = \max_{\|\mathbf{x}\|=1}\mathbf{x}^T\widetilde{\mathbf{S}}\mathbf{x}$ over all unit-norm column vectors $\mathbf{x}$. Now the output PSDs can be expressed as $\widetilde{S}_{pp} = \mathbf{x}^T\widetilde{\mathbf{S}}\mathbf{x}$ when $\mathbf{x} = [1,0]^T$ and $\widetilde{S}_{qq} = \mathbf{x}^T\widetilde{\mathbf{S}}\mathbf{x}$ when $\mathbf{x} = [0,1]^T$. Hence we conclude that the PSDs after any postfiber (as well as the PSDs before it) are sandwiched between the two eigenvalues: $\lambda_m \leqslant \widetilde{S}_{pp}, \widetilde{S}_{qq} \leqslant \lambda_M$, which therefore represent the envelopes shown as dashed curves in Fig. 12. Equality holds when the eigenvectors are $\mathbf{x} = [1,0]^T$ and $\mathbf{x} = [0,1]^T$, corresponding to a zero rotation angle $\theta = \hat{\theta} + \theta_p$ of the total rotation matrix $\mathbf{UV}$. We observe from Fig. 12 that by varying ξ_{post} one thus varies the frequencies of the minima–maxima of the PSDs, which satisfy the condition $\theta(\omega) = \hat{\theta}(\omega) + \xi_{post}\omega^2/2 = 0$.

Having characterized the effect of the postcompensating fiber on the received ASE PSDs, we now address the problem of finding the value of postcompensation that minimizes PG. The answer clearly depends on the modulation format, as already discussed in Section 2. In our cw model the modulation does not appear; hence we need a reasonable interpretation of the cw level. It has been shown[16] that the impact of signal modulation can be properly substituted by an equivalent reference cw level that accounts for an effective power within the memory time of the DM optical link. Once the proper power level has been
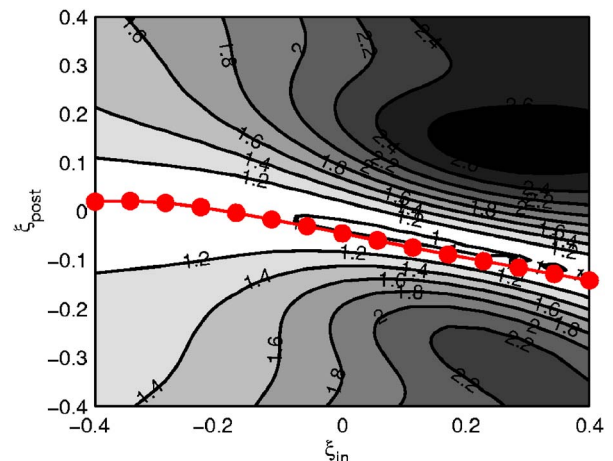
Fig. 13. (Color online) Normalized in-phase ASE variance versus ξ_{post} and ξ_{in}. Terrestrial long-span DM system with $S = 0.022$ and $\Phi_{NL} = 0.6\pi$. Circles: ξ_{post}^{opt} in Eq. (42).

identified, we observe that for on–off keying (OOK) modulation the best postcompensation choice minimizes the temporal variance of the in-phase ASE component, which is the main source of errors for an envelope-detector-based receiver.[6] Thanks to the closed-form expression of the ASE PSDs [Eqs. (29)], we quickly evaluated such a variance for a wide range of postcompensation and in-line compensation values. Figure 13 depicts the variance normalized to its value in the absence of PG. We used a system with $S = 0.022$ [corresponding to a fully compensated NRZ system at $R = 10$ Gb/s with $D_T = 8$ ps/(nm km)] and $\Phi_{NL} = 0.6\pi$. We evaluated the variance over a normalized bandwidth $B = 0.75$. The figure shows large tolerance to postcompensation errors for negative in-line dispersions, while for positive dispersions the tolerance is much reduced and the best region varies almost linearly with ξ_{in}. In the same figure we also plot a solid curve with circles corresponding to the ξ_{post}^{opt} that satisfies the condition $\theta(\omega = \pi) = 0$, which, using Eqs. (41) and (29), yields

$$\xi_{post}^{opt} = -\frac{1}{\pi^2}\arctan\left[\frac{c_1(\pi)r_r(\pi) + c_2(\pi)r_i(\pi)}{c_2(\pi)r_r(\pi) - c_1(\pi)r_i(\pi)}\right]. \quad (42)$$

Such a value of ξ_{post} forces the in-phase PSD $\widetilde{S}_{pp}$ to achieve its smallest possible value at frequency $f_n = 1/2$, i.e., near the center of the bulk of the OOK one-sided signal spectrum, thereby almost minimizing the variance of the in-phase ASE.

7. SYSTEM PERFORMANCE EVALUATION

An important issue with the small-signal PG model as applied to bit-error-rate (BER) computation is about its range of validity. For OOK systems at 10 Gb/s, although it is clear that at large end-line optical signal-to-noise ratio (OSNR) the small-signal assumption holds, but essentially no PG-induced sensitivity penalty can be observed at the receiver, it has been shown that, in 10 Gb/s ultralong terrestrial systems operating at low OSNR and thus employing forward error correction, a significant penalty due to PG can be observed, depending on the cumulated nonlinear phase and on the dispersion of the transmission fiber.[4,28] However, in such large PG cases the PSDs predicted by the small-signal PG model are inaccurate, and direct PSD estimation from simulations is necessary.[4,28]

For differential phase-shift keying (DPSK) systems at 10 Gb/s, matters are quite different. Already at relatively large OSNR values, significant PG-induced penalties can be observed even at moderate nonlinear phases,[16,23,29] and the small-signal PG model can thus be successfully used in performance evaluation.[30] While the standard BER computation goes through the evaluation of the phase noise statistics,[31] a method based on the assumption of a received colored Gaussian noise has been recently proposed.[16,30] Regarding the appropriateness of the cw assumption in deriving the ASE PSD, when the supporting pulses are return-to-zero (RZ) pulses such a PSD is not stationary, and it is unclear which cw level should be used to linearize the NLSE. Fortunately, it has been shown that it is possible to choose an equivalent cw level,
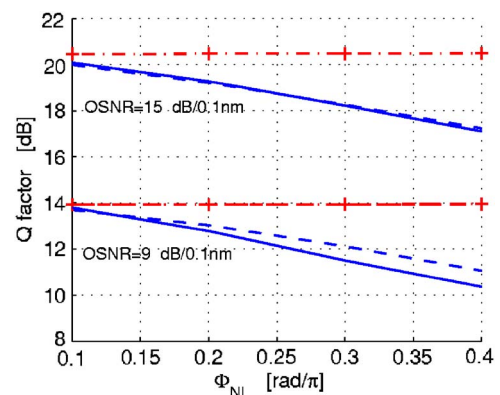
Fig. 14. (Color online) Q factor versus Φ_{NL} for a NRZ-DPSK signal after propagation into a 20×100 km fully compensated NZDSF$^+$ system at $R = 10$ Gb/s. Dashed curves: evaluation using formulas (29). Solid curves: evaluation using Monte Carlo PSDs. Dashed–dotted line with crosses: Q factor in the absence of PG.
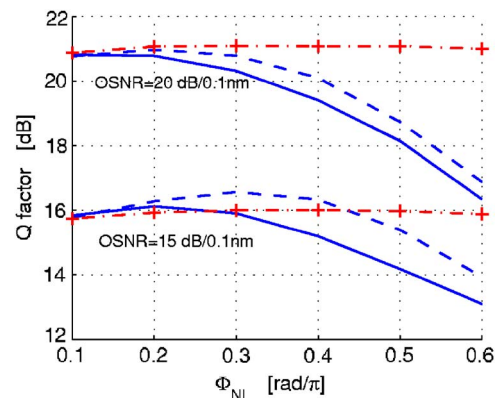
Fig. 15. (Color online) Q factor versus Φ_{NL} for a NRZ-OOK signal after propagation into a 20×100 km fully compensated NZDSF$^+$ system at $R = 10$ Gb/s. Dashed curves: evaluation using formulas (29). Solid curves: evaluation using simulated PSDs. Dashed–dotted lines with crosses: Q factor in the absence of PG.

which depends on the details of the DM map, so that the cw small-signal model yields correct results even for RZ pulses.[16]

In this section we will provide numerical examples of performance evaluation in both DPSK and OOK systems that further support the above observations. All results presented next will refer to a single-channel transmission.

Figure 14 shows the Q factor versus average nonlinear phase for an NRZ-DPSK 20×100 km fully compensated NZDSF$^+$ system at $R = 10$ Gb/s ($S = 0.008$) working at an end-line OSNR of either 15 or 9 dB/0.1 nm. Before transmission, a precompensation of –44 ps/nm was used, whereas after the link the postcompensation was 420 ps/nm. Before detection a Gaussian optical filter of bandwidth $1.8R$ removed the out-of-band noise. In all cases the Q factor was obtained by inverting the BER evaluated through a Karhunen–Loéve method for quadratic receivers.[16] The solid curves represent the Q factor obtained from the true PSDs estimated from SSFM simulations.[4] The dashed curves represent the Q factor obtained by using our theoretical PSDs [Eqs. (29)], and the dashed–dotted line with crosses represents the Q fac-

tor in the absence of PG, which clearly shows the absence of signal distortion within the shown range of nonlinear phases. With the inclusion of PG, we see that performance quickly degrades with increasing nonlinear phase and that the linear PG model gives an accurate prediction of the performance at OSNR = 15 dB. At a low OSNR = 9 dB, the prediction is still accurate up to $\Phi_{NL} = 0.2\pi$, i.e., up to Q factor penalties of about 1 dB. We note that PG significantly affects the performance already at small Φ_{NL}. This is due to the quadrature noise component, which is the main source of errors for DPSK and which is always more inflated by PG than the in-phase component over the signal bandwidth.

Figure 15 shows the Q factor versus average Φ_{NL} for the same DM system as above but now for a 10 Gb/s NRZ-OOK signal and at an end-line OSNR of either 15 or 20 dB/0.1 nm. The postcompensation was 220 ps/nm. Owing to the nonstationary nature of noise, in the BER evaluation we adopted a simplified model that adds PG only during marks.[4] Since the map strength was small, in Eqs. (29) we used as the cw power level the transmitted peak power, which for a fixed average Φ_{NL} is twice that of DPSK. From Fig. 15 we note that at OSNR = 20 dB the Q factor obtained from the theoretical PSDs overestimates the one using the simulated PSDs by at most 0.7 dB, whereas at OSNR = 15 dB the overestimation can exceed 1 dB. Moreover, at OSNR = 15 dB the linear model predicts an unrealistic performance improvement around $\Phi_{NL} = 0.3\pi$ over the zero-PG case due to squeezing of the in-phase component. Note that, as opposed to DPSK, for OOK the main source of errors is the in-phase ASE component, which, especially in the smallest OSNR case, is strongly inflated at large Φ_{NL} by the quadratic and higher-order ASE terms that are neglected by the linear PG model.[4]

8. CONCLUSIONS

In this paper we derived several fundamental scaling laws that govern the mechanism of parametric gain in dispersion-managed periodic links. Having in mind non-soliton signal transmissions, we focused on systems working at limited cumulated nonlinear phase and in-line dispersion. Beside such two system parameters, we showed that, for realistic dispersion maps dominated by fiber loss, only a third parameter—the (first-order) map strength S—is necessary to completely describe the spectral properties of PG up to frequencies of the order of the inverse of the square root of S. We also provided the relation of our strength S with the strength definition used in soliton communications. For mathematical tractability, our PSD formulas were derived for systems with infinitely many spans, but the results approximately hold for nonlinear phase rotations per span smaller than roughly 0.1 rad. We emphasized the fundamental role of the DM kernel in determining the DM system's small-signal response, although the kernel is known to completely determine even the large-signal response.[17] For instance, we proved that the system eigenvalues solely depend on the kernel absolute value, so that modulation instability can exist only at positive in-line dispersion. We also gave a general rule to determine when dispersion management can provide sub-

stantially different ASE PSDs with respect to an unmapped system. The limited role of dispersion slope was discussed, and it was found that it hardly affects the ASE PSDs, in line with similar results for unmapped systems.[7] The impact of a postcompensation fiber at the end of the DM link was also discussed, with emphasis on the key role of the PSD matrix eigenvalues, which represent the envelope of the in-phase and quadrature PSDs for all possible values of the postfiber dispersion. Such an interpretation eases the search for an optimal value of postcompensation to minimize PG. Finally, we provided examples of application of the PG linear model to system performance evaluation, and we showed that, while the model can be overly optimistic for OOK systems, its predictions of DPSK are, instead, quite reliable.

This work can be extended in several directions. For instance, an issue of practical interest is the inclusion of the effect of random longitudinal variations of the zero-dispersion wavelength along the DM line, a topic already investigated for the four-wave-mixing effect.[32] Such fluctuations make the optical link aperiodic, thus violating a fundamental assumption of the DM-NLSE. In this case, one could follow the approach of Ablowitz and Moeser,[33] where the averaging operation implied in the kernel derivation [expression (8)] is now taken over the entire link. Another interesting extension is the case of multiple cw pumps with broadband ASE, a topic already tackled in the non-DM case.[14,34]

ACKNOWLEDGMENTS

P. Serena, the corresponding author, can be reached by e-mail at serena@tlc.unipr.it.

REFERENCES AND NOTES

1. G. P. Agrawal, *Nonlinear Fiber Optics* (Academic, 2001).
2. R. Holzlöhner, V. S. Grigoryan, C. R. Menyuk, and W. L. Kath, "Accurate calculation of eye diagrams and bit error rates in optical transmission systems using linearization," J. Lightwave Technol. **20**, 389–400 (2002).
3. B. Xu and M. Brandt-Pearce, "Optical fiber parametric-gain-induced noise coloring and amplification by modulated signals," J. Opt. Soc. Am. B **21**, 499–513 (2004).
4. P. Serena, A. Bononi, J. C. Antona, and S. Bigo, "Parametric gain in the strongly nonlinear regime and its impact on 10-Gb/s NRZ systems with forward-error correction," J. Lightwave Technol. **23**, 2352–2363 (2005).
5. A. Carena, V. Curri, R. Gaudino, P. Poggiolini, and S. Benedetto, "New analytical results on fiber parametric gain and its effects on ASE noise," IEEE Photon. Technol. Lett. **9**, 535–537 (1997).
6. R. Hui, M. O'Sullivan, A. Robinson, and M. Taylor, "Modulation instability and its impact in multispan optical amplified IMDD systems: theory and experiments," J. Lightwave Technol. **15**, 1071–1082 (1997).
7. C. Lorattanasane and K. Kikuchi, "Parametric instability of optical amplifier noise in long-distance optical transmission systems," IEEE J. Quantum Electron. **33**, 1068–1074 (1997).
8. M. Karlsson, "Modulation instability in lossy optical fibers," J. Opt. Soc. Am. B **12**, 2071–2078 (1995).

9. F. Matera, A. Mecozzi, M. Romagnoli, and M. Settembre, "Sideband instability induced by periodic power variation in long-distance fiber links," Opt. Lett. **18**, 1499–1501 (1993).

10. N. J. Smith and N. J. Doran, "Modulation instabilities in fibers with periodic dispersion management," Opt. Lett. **21**, 570–572 (1996).

11. M. Midrio, P. Franco, and M. Romagnoli, "Noise statistics in transmission systems with grating dispersion compensation," J. Opt. Soc. Am. B **15**, 2748–2756 (1998).

12. E. Ciaramella and M. Tamburrini, "Modulation instability in long amplified links with strong dispersion compensation," IEEE Photon. Technol. Lett. **11**, 1608–1610 (1999).

13. C. J. McKinstrie, S. Radic, and A. R. Chaplyvy, "Parametric amplifiers driven by two pump waves," IEEE J. Sel. Top. Quantum Electron. **8**, 538–547 (2002).

14. J. M. Chávez Boggio, S. Tenenbaum, and H. L. Fragnito, "Amplification of broadband noise pumped by two lasers in optical fibers," J. Opt. Soc. Am. B **18**, 1428–1435 (2001).

15. F. Consolandi, C. De Angelis, A.-D. Capobianco, and A. Tonello, "Parametric gain in fiber systems with periodic dispersion management," Opt. Commun. **208**, 309–320 (2002).

16. P. Serena, A. Orlandini, and A. Bononi, "Parametric-gain approach to the analysis of single-channel DPSK/DQPSK systems with nonlinear phase noise," J. Lightwave Technol. **24**, 2026–2037 (2006).

17. M. J. Ablowitz and T. Hirooka, "Managing nonlinearity in strongly dispersion-managed optical pulse transmission," J. Opt. Soc. Am. B **19**, 425–439 (2002).

18. A. Papoulis, *Probability, Random Variables, and Stochastic Processes*, 3rd ed. (Mc-Graw-Hill, 1991).

19. D. Zwillinger, *Handbook of Differential Equations* (Academic, 1998).

20. H. A. Haus, "Quantum noise in a solitonlike repeater system," J. Opt. Soc. Am. B **8**, 1122–1126 (1991).

21. L. C. Evans, "An introduction to stochastic differential equations," http://math.berkeley/edu/~evans/.

22. C.-T. Chen, *Linear System Theory and Design* (Holt-Saunders, 1984), pp. 49–50.

23. J.-P. Gordon and L. F. Mollenauer, "Phase noise in photonic communications systems using linear amplifiers," Opt. Lett. **15**, 1351–1353 (1990).

24. J. C. Bronski and J. N. Kutz, "Modulation stability of plane waves in nonreturn-to-zero communications systems with dispersion management," Opt. Lett. **21**, 937–939 (1996).

25. M. J. Ablowitz, T. Hirooka, and T. Inoue, "Higher-order analysis of dispersion-managed transmission systems: solutions and their characteristics," J. Opt. Soc. Am. B **19**, 2876–2885 (2002).

26. A comparison of DM systems with different span lengths at a constant nonlinear phase can make sense, for instance, in a metropolitan network environment where, although the fiber links are short, a big lumped loss, such as a demultiplexer or an add–drop module, is inserted at the end of each span connecting two consecutive nodes.

27. R. A. Horn and C. R. Johnson, *Matrix Analysis* (Cambridge U. Press, 1999).

28. A. Bononi, P. Serena, J.-C. Antona, and S. Bigo, "Implications of nonlinear interactions of signal and noise in low-OSNR transmission systems with FEC," in *Optical Fiber Communication Conference*, OSA Trends in Optics and Photonics Series (Optical Society of America, 2005), paper OTHW5.

29. H. Kim and A. H. Gnauck, "Experimental investigation of the performance limitation of DPSK systems due to nonlinear phase noise," IEEE Photon. Technol. Lett. **15**, 320–322 (2003).

30. A. Orlandini, P. Serena, and A. Bononi, "An alternative analysis of nonlinear phase noise impact on DPSK systems," in *Proceedings of the IEEE European Conference on Optical Communication* (IEEE, 2006), paper Th3.2.6.

31. K.-P. Ho, "Probability density of nonlinear phase noise," J. Opt. Soc. Am. B **20**, 1875–1879 (2003).

32. E. Ciaramella, "Effect of non-uniform chromatic dispersion fibre link in determining system limitations due to four wave mixing," Electron. Lett. **34**, 202–204 (1998).

33. M. J. Ablowitz and J. Moeser, "Dispersion management for randomly varying optical fibers," Opt. Lett. **8**, 821–823 (2004).

34. G. Bosco, A. Carena, V. Curri, R. Gaudino, P. Poggiolini, and S. Benedetto, "Parametric gain in multiwavelength systems: a new approach to noise enhancement analysis," IEEE Photon. Technol. Lett. **9**, 1135–1137 (1999).